

Multimodal Fusion of EMG and Vision for Human Grasp Intent Inference in Prosthetic Hand Control

Mehrshad Zandigohar, Mo Han, Mohammadreza Sharif, Sezen Yağmur Günay, Mariusz P. Furmanek, Mathew Yarossi, Paolo Bonato, Cagdas Onal, Taşkın Padır, Deniz Erdoğan, Gunar Schirner

Abstract—Objective: For lower arm amputees, robotic prosthetic hands promise to regain the capability to perform daily living activities. Current control methods based on physiological signals such as electromyography (EMG) are prone to yielding poor inference outcomes due to motion artifacts, muscle fatigue, and many more. Vision sensors are a major source of information about the environment state and can play a vital role in inferring feasible and intended gestures. However, visual evidence is also susceptible to its own artifacts, most often due to object occlusion, lighting changes, etc. Multimodal evidence fusion using physiological and vision sensor measurements is a natural approach due to the complementary strengths of these modalities. Methods: In this paper, we present a Bayesian evidence fusion framework for grasp intent inference using eye-view video, eye-gaze, and EMG from the forearm processed by neural network models. We analyze individual and fused performance as a function of time as the hand approaches the object to grasp it. For this purpose, we have also developed novel data processing and augmentation techniques to train neural network components. Results: Our results indicate that, on average, fusion improves the instantaneous upcoming grasp type classification accuracy while in the reaching phase by 13.66% and 14.8%, relative to EMG and visual evidence individually, resulting in an overall fusion accuracy of 95.3%. Conclusion: Our experimental data analyses demonstrate that EMG and visual evidence show complementary strengths, and as a consequence, fusion of multimodal evidence can outperform each individual evidence modality at any given time.

Index Terms—Dataset, EMG, Grasp Detection, Neural Networks, Robotic Prosthetic Hand.

I. INTRODUCTION

IN 2005, an estimated of 1.6 million people (1 out of 190 individuals) in the US were living with the loss of a limb [1]. This number is expected to double by the year 2050. The most common prosthesis in upper extremity amputees is cosmetic hand type with the prevalence of 80.2% [2]. As limb loss usually occur in the working ages, dissatisfaction in the effectiveness of the prescribed prosthesis, will often

P. Bonato is with the Motion Analysis Lab at Spaulding Rehabilitation Hospital; C. Onal is with the Soft Robotics Lab at Worcester Polytechnic Institute; the rest of the authors are with the Electrical and Computer Engineering department at Northeastern University.

Correspond to G. Schirner of Electrical and Computer Engineering, Northeastern University, Boston, MA, 02120 USA (email: schirner@ece.neu.edu).

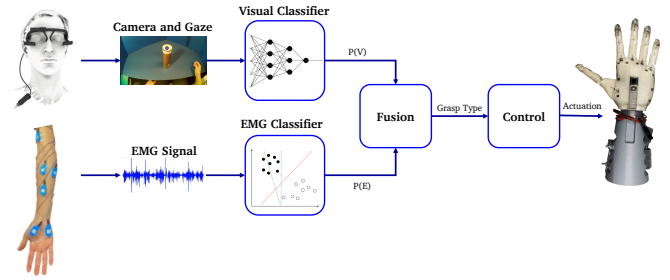


Fig. 1: Proposed System Overview (eye-tracker from [8]).

impose difficulties in an amputee's personal and professional life. Therefore, providing a functional prosthesis is critical to address this issue and can improve quality of life for amputees.

There has been numerous efforts in the field to meet amputees' high expectations for intuitive control of a powered prosthesis, especially methods based on inferring the human's intent using the amputee's body signals e.g., Electroencephalography (EEG) and Electromyography (EMG) signals [3]–[5]. Despite the advances in the control of robotic prosthetic hands using physiological signals, current control methods generally lack robustness which reduces their effectiveness in amputees' daily life activities. Reliance solely on human input, e.g. physiological signals from the amputee including EEG and EMG, has many drawbacks that will adversely impact the performance of the prosthetic hand. These include artifacts caused by electrode shifting, changes of skin electrode impedance over time, muscle fatigue, cross-talk between electrodes, stump posture change, and the need for frequent calibration [6], [7]. Therefore, there is a need for new sources of information to provide more robust control of the robotic hand.

Another major source of information in the state-of-the-art methods are RGB cameras which are usually bundled with a control method based on pattern recognition or deep neural networks. These methods generally use this information to infer the reaching trajectory, time of triggering the grasp or most importantly, the grasp used to control the finger movements of the robotic hand [9], [10]. Similar to grasp classification using EEG/EMG evidence, solely relying on visual data is susceptible to several artifacts including object occlusion, lighting changes, and many more.

To increase the robustness of grasp classification, we propose fusing the evidence from amputee's physiological signals with the physical features evident in the visual data from the camera. As presented in Figure 1, the proposed system design consists of a neural visual classifier to detect and provide probabilities of grasp gestures given world imagery and eye-gaze from the eye tracking device; an EMG classifier predicting the EMG evidence from amputee's forearm; and a Bayesian evidence fusion framework to fuse the two. The selected gesture is then utilized by the robotic controller to actuate the fingers. Our experimental results show that fusion can outperform each of the individual EMG and visual classification methods at any given time. More specifically, fusion improves the average grasp classification accuracy during reaching by 13.66%, and 14.8% for EMG and visual classification respectively with the total accuracy of 95.3%. Moreover, such utilization of fusion allows the robotic hand controller to deduce the correct gesture in a more timely fashion, hence, additional time is left for the actuation of the robotic hand. All classification methods were tested on our custom dataset with synchronized EMG and imagery data. The main contributions of this work are:

- **Synchronized grasp dataset:** We collected a multimodal dataset for prosthetic control consisting of imagery, gaze and dynamic EMG data, from 5 subjects using state-of-the-art sensors, all synchronized in time.
- **Grasp segmentation and classification of dynamic EMG:** We segmented the non-static EMG data into multiple dynamic motion sequences with an unsupervised method, and implemented gesture classification based on the dynamic EMG.
- **Visual grasp detection:** We built a CNN classifier capable of detecting gestures in visual data, and background generalization using copy-paste augmentation.
- **Robust grasp detection:** We implemented the multimodal fusion of EMG and imagery evidence classifications, resulting in improved robustness and accuracy at all times.

The rest of this paper continues as follows: section II provides details on system setup and data collection protocols. After that, section III provides an in-depth study of EMG phase segmentation and gesture classification. Then, section IV discusses visual detection and generalization methods. section V provides fusion formulation and results, and lastly, we summarize our developments and discuss future directions in the section VI.

II. SYSTEM SETUP

This section provides the technical details required to replicate the data acquisition system and results. The details are provided in four subsections: 1) system overview, 2) sensor configurations, 3) experiment protocol, and 4) data collection.

A. System Overview

Our data acquisition system entails collecting, synchronizing, and storing information from subject's eye-gaze, surface EMG, and an outward facing world camera fixed to the

eye-glass worn eye-tracker. Robot Operating System (ROS) enabled the communication framework. ROS Bag file format was used to store the data on disc.

A mobile binocular eye-tracker (Pupil Core headset, Pupil-Lab, Germany) with eye facing infrared cameras for gaze tracking and a world facing RGB camera was used. The gaze accuracy and precision were 0.60° and 2%, respectively. The gaze detection latency was at least 11.5 ms according to the manufacturer. The world camera of the eye-tracker recorded the work-space at 60Hz@720p and FOV of $99^\circ \times 53^\circ$. The gaze and world camera data were sent to ROS in real-time using ZeroMQ [11].

Muscle activity was recorded from subjects' right forearm through 12 Z03 EMG pre-amplifiers with integrated ground reference (Motion Lab Systems, Baton Rouge, LA, USA). The pre-amplifiers provided x300 gain and protection against electrostatic discharge (ESD) and radio-frequency interference (RFI). The signals were passed to two B&L 6-channel EMG electrode interfaces (BL-EMG-6). Then, an ADLINK USB 1902 DAQ was used to digitize EMG data, which was then stored along with other signals in the ROS Bag file. The ADLINK DAQ used a double-buffer mechanism to convert analog signals. Each buffer was published to ROS when full. The system components are depicted in Figure 2 (a).

B. Sensor Configurations

1) *Eye-tracker Configuration:* The orientation of the eye and world cameras were adjusted at the beginning of the experiment for each subject and remained fixed during the whole experiment. A single marker calibration method leveraging the vestibulo-ocular reflex (VOR) was used to calibrate the gaze tracker. While gazing at the marker lying on the table, the subject moved their head slowly to cover the whole field of view.

2) *EMG Sensor Configuration:* Surface EMG was recorded at $f = 1562.5$ Hz in $C = 12$ muscles of the arm, forearm and hand in order to capture dynamic hand gesture information and arm movement: First Dorsal Interosseous (FDI), Abductor Pollicis Brevis (APB), Flexor Digiti Minimi (FDM), Extensor Indicis (EI), Extensor Digitorum Communis (EDC), Flexor Digitorum Superficialis (FDS), Brachioradialis (BRD), Extensor Carpi Radialis (ECR), Extensor Carpi Ulnaris (ECU), Flexor Carpi Ulnaris (FCU), Biceps Brachii-Long Head (BIC), and Triceps Brachii-Lateral Head (TRI). The muscle locations were found by palpation during voluntary arm movements. After skin preparation, the surface electrodes were fixed to the skin overlying each muscle using tape.

C. Experiment Protocol

The experiment included moving objects among cells of an imaginary 3×2 grid with pre-defined gestures. The experimental setup is shown in Figure 2 and the pre-defined gestures are shown in Figure 3. The experiment was comprised of two sessions. In the first session, subjects moved objects in a clockwise manner, and in the second session objects were moved in a counter-clockwise manner (only the clockwise session is demonstrated in Figure 2). Having two sessions

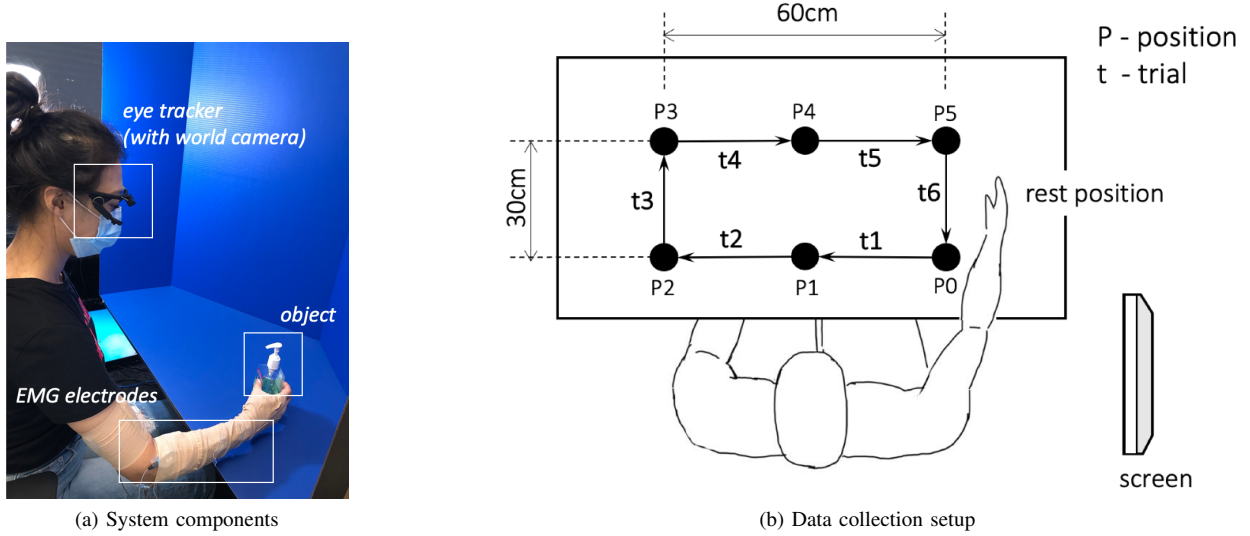


Fig. 2: System components and data collection setup. Only the clockwise session is demonstrated in (b).

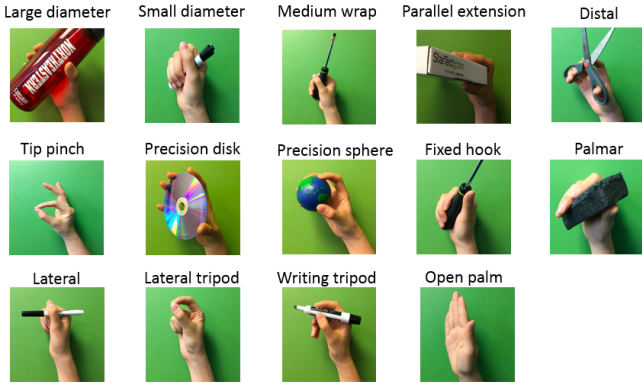


Fig. 3: Selected 14 gestures for the classification problem.

contributed to the diversity of the dataset for the EMG signal and the camera image patterns.

In each session, 54 objects were placed on a table one by one within the reach of the subjects so they could locate it on the proper spot before the experiment began. Then, for each object, an image was shown on the monitor on the right side of the subject instructing them how to grasp the object. Then, the moving experiment started. Audio cues, i.e. short beep sounds, were used to trigger each move.

The subject performed 6 trials for each object, where each trial was executed along its corresponding predefined path, as shown in Figure 2 (b). During the first trial t_1 , the object was moved from the initial position P_0 to the position P_1 , followed with another five trials to move the object clockwise until it was returned to the initial position P_0 , leading to 6 trials in total. After moving all objects in the clockwise order, the second session of counterclockwise started after a 15-minute break. The break meant to help the subject refresh and to maintain focus on the task in the second session. The interval between consecutive audio cues was set to 4 seconds for all objects. The entire experiment for the 6 trials per object, i.e. moving one object around the rectangle, took about 37 seconds

including the instructions.

D. Data Collection

Experimental data were collected from 5 healthy subjects (4 male, 1 female; mean age: 26.7 ± 3.5 years) following institutionally approved informed consent. All subjects were right-handed and only the dominant hand was used for the data collection. None of the subjects had any known motor or psychological disorders.

Feix et al. [12] proposed that human grasp taxonomy consists of 33 classes if only the static and stable gestures are taken into account. The human hand has at least 27 degrees of freedom (DoF) to achieve such a wide range of gestures; however, most existing prosthetic hands do not have this many DoF [13]. Therefore, in our work, the experimental protocol was focused on those 14 representative gestures involving commonly used gestures and wrist motions [12]. As shown in Figure 3, the 14 classes were: large diameter, small diameter, medium wrap, parallel extension, distal, tip pinch, precision disk, precision sphere, fixed hook, palmar, lateral, lateral tripod, writing tripod, and open palm/rest. In our classification problem, we mapped the 14 gestures with 14 gesture labels $l \in \{0, 1, \dots, 13\}$, where $l = 0$ was defined as open-palm/rest gesture and $l \in \{1, \dots, 13\}$ were accordingly identified as the other 13 gestures in the order listed in Figure 3.

III. CLASSIFICATION OF EMG EVIDENCE

Extracting user hand/arm motion instructions from EMG signals has been widely utilized for human-robot interactions. A major challenge of online interaction with robots is the reliability of EMG recognition from real-time data. In this section, we introduce our method for the EMG control of the robotic hand. We propose a framework for classifying our collected EMG signals generated from continuous grasp movements with variations in dynamic arm/hand postures. We first utilized an unsupervised segmentation method to segment

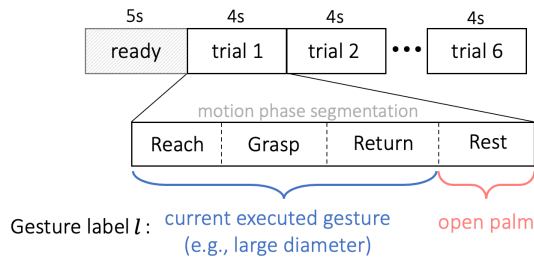


Fig. 4: Experiment timeline. The subject was given 5 seconds to read the shown gesture before the first trial. Each trial lasted for 4 seconds, repeated for 6 trials without interruption. All EMG trials were segmented unsupervisedly into four sequences of reaching, grasping, returning and resting. The first three motion phases were labeled as gesture $l \in \{1, \dots, 13\}$ corresponding to the target object, and the resting phase was tagged by the open-palm label $l = 0$.

the EMG data into multiple motion states, and then constructed a classifier based on those dynamic EMG data.

A. EMG Data Pre-Processing

The data were filtered with a band-pass Butterworth filter of 40-500 Hz, where the high pass serves to remove motion artifact and the low pass is used for anti-aliasing and removal of any high frequency noise outside of the normal EMG range. Afterwards the root-mean-square envelopes [14] of the EMG signal were constructed using a sliding window of length 150 samples. A maximum voluntary contraction (MVC) test was manually performed for each muscle at the beginning of the recordings. During the test, the subjects were instructed to perform isometric contractions constantly for each muscle [15]. Finally, the resulting EMG envelopes were normalized to the maximum window value of MVC data, which were processed the same as the task data. The processed EMG signals were further divided into sliding windows of $T = 320$ ms, with a delay of 32 ms between two consecutive windows. Both feature extraction and classification were conducted based on each sliding window.

B. EMG Feature Extraction

Features of EMG in the time domain can be extracted based on the raw EMG time series in real-time without any transformation, and require lower computational complexity compared with other features [16]. Three time domain features were adopted in this work, including root mean square (RMS), mean absolute value (MAV), and variance of EMG (VAR) [16]. The RMS feature represents the square root of the average power of the EMG signal for a given period of time, which models the EMG amplitude as a Gaussian distribution. MAV feature is an average of absolute value of the EMG signal amplitude, which indicates the area under the EMG signal once it has been rectified [4]. VAR feature is defined as the variance of EMG, which is calculated as an average of square values of the deviation of the signal from the mean.

The input for the feature extraction is the pre-processed EMG window $X \in \mathbb{R}^{C \times T}$, where $C = 12$ is the channel

number of EMG from all muscles and $T = 320$ ms is the window length with a sampling rate of $f = 1562.5$ Hz. For each input EMG window $X \in \mathbb{R}^{C \times T}$, we extracted all the three mentioned time-domain features leading to an output feature vector of $Z \in \mathbb{R}^{3C \times 1}$.

C. Data Annotation

In order to approach the gesture classification in a continuous manner, each EMG trial was assumed to include 4 different movement sequences, i.e. reaching, grasping, returning and resting. The proposed motion sequences are naturally and commonly performed actions by human during the reach-to-grasp movements, giving greater probability to intent transitions that are likely to follow one another, such as a “grasp” action is always following a “reach” movement and followed by a “return” action. In our method, as shown in Figure 4, we first segmented each EMG trial unsupervisedly into 4 sequences, and then labeled them separately with gesture label l according to the specific motion. During each trial, the dynamic grasp movements were performed naturally by the subject without limitation on the timing of each motion phase, so the length of each phase is not necessarily equal.

1) Unsupervised EMG Segmentation of Dynamic Motion:

The EMG trial from dynamic grasp movement was segmented using an unsupervised method of Greedy Gaussian Segmentation (GGS) [17], based on the assumption that EMG signal under a specific stationary status can be well modeled as a zero-mean random process which is Gaussian distributed [18]. The GGS method was proposed to solve the problem of breaking multivariate time series into segments over which the data is well explained as independent samples from different Gaussian distributions corresponding to each segment. GGS assumes that, in each segment, the mean and covariance are constant and unrelated to the means and covariances in all other segments. The problem was formulated as a maximum likelihood problem, which was further reduced to a optimization task of searching over the optimal breakpoints leading to the overall maximum likelihood from all Gaussian segments. The approximate solution of the optimized segments was computed in a scalable and greedy way of dynamic programming, by adding one breakpoint in each iteration and then adjusting all the breakpoints to approximately maximize the objective.

In order to formulate four segments corresponding to the four grasp motion phases (reaching, grasping, returning and resting), we assigned three breakpoints to each EMG trial. Practically each of the four dynamic phases may not be strictly steady-state, but we nevertheless encode such transitions from one intent to another based on the proposed motion sequences considering the inherent stochastic nature of EMG signals. We then utilized the GGS algorithm to locate the locally optimal segment boundaries given the specific number of segments. The obtained three optimal segment boundaries led to four EMG sequences, where each of the four sequences was modeled as an independent 12-channel multivariate Gaussian distribution with different means and variances.

2) Hand Gesture Annotation of EMG: In order to classify gestures from dynamic EMG signals in a real-time manner, following the motion phase segmentation, the resulting EMG segments were further annotated by a group of gesture label $l \in \{0, 1, \dots, 13\}$, where $l = 0$ was defined as open-palm/rest gesture and $l \in \{1, \dots, 13\}$ were accordingly identified as the other 13 gestures listed in Figure 3.

During the reach-to-grasp movement, the configuration of the fingers and wrist changes simultaneously and continuously with the arm's motion according to the shape and distance of the target object [19]. For example, humans tend to pre-shape their hands before they actually touch the target object during a grasp, and this formation of the limb before the grasp is in direct relation with the characteristics of the target object [19]. Therefore, to accomplish a smooth interpretation of the grasping gesture, as presented in Figure 4, we annotated unsupervisedly segmented sequences of reaching, grasping and returning as the executed gesture $l \in \{1, \dots, 13\}$ corresponding to the target object, and tagged the resting phase with the open-palm label $l = 0$.

D. Gesture Classification of Dynamic EMG

We constructed a model for classifying the gesture $l \in \{0, 1, \dots, 13\}$ of dynamic EMG signals with corresponding data pairs of $\{(X_i, l)\}_{i=1}^n$, where $X_i \in \mathbb{R}^{C \times T}$ is the i th EMG window with channel number $C = 12$ and window length $T = 320$ ms of $f = 1562.5$ Hz sampling rate, and n is the total number of windows. For each EMG window $X_i \in \mathbb{R}^{C \times T}$, three time-domain features of RMS, MAV and VAR were extracted as $Z_i \in \mathbb{R}^{3 \times 1}$, leading to data pairs of $\{(Z_i, l)\}_{i=1}^n$, which were the final inputs to train the grasp-type classifier.

We utilized the extra-trees method [20] as the classifier, which is an ensemble method that incorporates the averaging of various randomized decision trees on different sub-samples of the dataset to improve the model performance and robustness. The number of trees in the extra-trees forest was set to be 50 in this work, and the minimum number of samples required to split an internal node was set as 2.

E. Experimental Evaluations on Dynamic-EMG Classification

1) Training and Validation: We performed inter-subject training and validation for the 14-class gesture classification of dynamic EMG. The classification analyse was implemented through a left-out validation protocol. For each subject, the collected 6 EMG trials of each object in Figure 2 (b) were randomly divided into training set (4 trials) and validation set (2 trials), leading to 224 training trials (66.7%) and 112 validation trials (33.3%) in total for each subject. The classifier was only trained on the training set while validated on the validation set which was unseen to the model. We validated the pre-trained model on each entire EMG trial (including four phases of reaching, grasping, returning and resting) from the validation set, whereas we trained the model only with reaching, grasping and resting phases in each EMG trial of the training set. Since our main goal is to decode the grasping

intention and pre-shape the robotic hand at an earlier stage of reach-to-grasp motion before the final grasp accomplished, we therefore excluded the EMG data of returning phase during training to reduce the distraction of the model from the phase where the hand already released the object.

2) Time-Series Alignment: As shown in Figure 6, time series of all validation trials were aligned with the beginning of the grasping phase, which was marked as 0ms in the timeline. The overall evaluated performance of the model was averaged over the performances of all validation trials based on the given aligned timeline. The four dynamic phases were freely performed by the subject, leading to their different lengths. Therefore, aligning the validation time series with the grasping phase during the performance average concentrated the assessment more on the central region between reaching and grasping phases, which were the most important phases for decision making. This resulted in more orderly time series, which were more relevant to the dynamic validation of overall performance.

As illustrated in Figure 6, each validation trial was shifted backward 700ms (around half the length of entire resting phase), for presenting the resting phase from last trial in front of the reaching phase of current trial, to show the dynamic performance transition between the two movement phases.

3) Results: Performance of the dynamic-EMG classifier was evaluated by two metrics - the predicted probabilities and the accuracy on validation set, which are presented in Figure 5 as functions of time. Each time point in Figure 5 represents a EMG window and both metrics were averaged based on each time window over the validation set. The breakpoints between different motion phases (represented by vertical dashed lines) were also averaged across validation trials. In Figure 5 (a), the predicted probability is defined as the output probability of the classifier corresponding to each class, and here we show the probabilities of grasp gesture, rest gesture and top competitor. The grasp gesture is defined as the executed true gesture during the non-resting phases, the rest gesture represents the open-palm/rest gesture, and the top competitor is identified as the most possible gesture except for the grasp gesture and the rest gesture. In Figure 5 (b), the corresponding accuracy curves of successfully detecting the grasp gesture and rest gesture are displayed, where the accuracy is defined as the frequency of appearance of a specific label with the maximum probability over the output probability distribution.

As illustrated in Figure 5 (a), the predicted probability of the grasp gesture $l \in \{0, 1, \dots, 13\}$ increased steadily during the reach-to-grasp movement when the grasp was carried out from the resting status, reaching its peak in the grasping phase, and then gradually decreased when subject finished the grasp and returned to resting status again. Simultaneously, the predicted probability of rest gesture first reduced dramatically to the value lower than 0.2 as the grasp movement happened, until the hand returned to the resting position when the open-palm probability progressively went up again. In addition, the predicted probability of the top competitor was remained stably lower than 0.2. The first intersection of predicted grasp-gesture and rest-gesture probability curves indicates the point when the grasp-gesture decision outperforms the rest-gesture

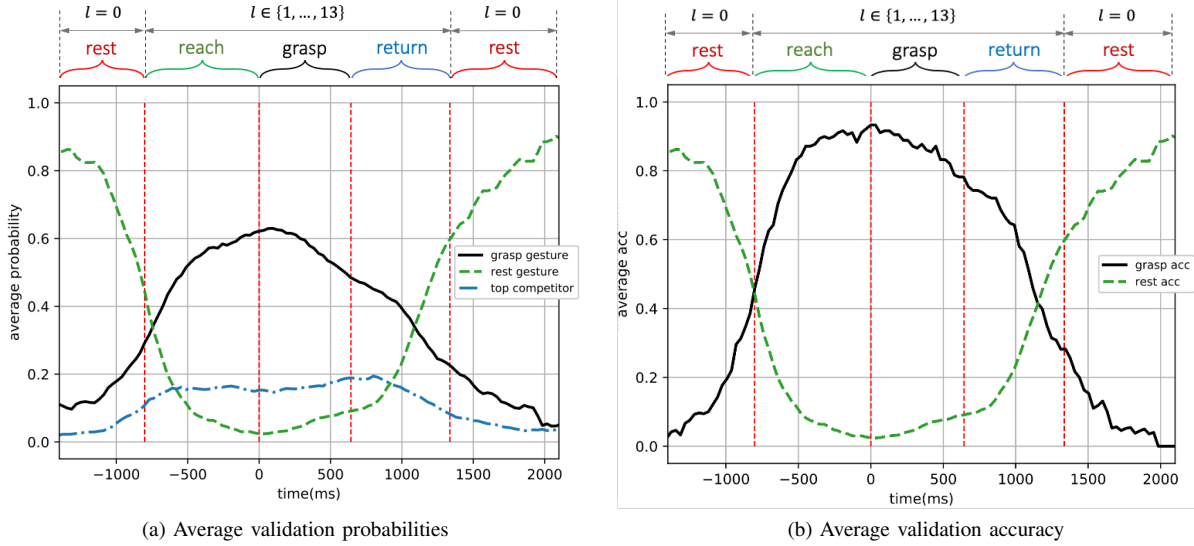


Fig. 5: The performance on the validation set of the dynamic-EMG gesture classifier. The grasp gesture is defined as the executed true gesture during the non-resting phases, the rest gesture represents the open-palm/rest gesture during the resting phase, and the top competitor is identified the most possible gesture except for the executed true gesture and the rest gesture.

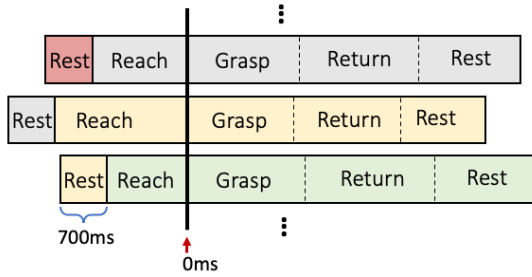


Fig. 6: The time series alignment for different trials.

decision. Ideally, this intersection is expected to appear right at the junction where the resting phase ends and the reaching phase starts in order to indicate the beginning of the hand motion. However, in practice, the hand movement could only be predicted based on the past motion, and such motion first starts from the reaching phase. So the intersection is expected to be observed after the start point of the reaching phase, but the closer to this start point, the better. In Figure 5 (a), the first intersection of the two curves appears $> 700\text{ms}$ earlier than the start of the grasping phase, which is after but very close to the beginning of the reaching phase and allows enough time to pre-shape the robotic hand before the actual grasp.

As shown in Figure 5 (b), for the grasp gesture classification, the averaged accuracy was higher than 80% throughout most of the reaching and grasping phases, which are the most critical phases for making robotic-grasp decision. The average accuracy during resting phase were also highly accurate and sensitive to perform as a detector to trigger the robotic grasp as shown in Figure 5 (b). In between dynamic phases of resting and non-resting, the accuracy also shows a smooth transition. It is worth noting that the validation accuracy was still higher than 75% at the beginning of the returning phase even though the model was not trained on any data from that

phase, illustrating the generalization and robustness of our model on dynamic EMG classification.

IV. VISUAL GESTURE CLASSIFICATION

As mentioned earlier, visual grasp detection does not rely on the amputee's physiological signals, and therefore can provide more robustness to the system than EMG alone. Despite this major advantage, there are known challenges to classification and detection from visual data using deep learning. More specifically, the classifier needs to be invariant to environment changes such as the lighting, background, camera rotation and noise. Moreover, in the case of grasp detection, the final decision should be invariant to the object's color.

To face these challenges, we utilize training with data augmentation techniques. Using the aforementioned set of data, a state-of-the-art pretrained object detector is fine-tuned for the purpose of grasp detection. The grasp detector then provides bounding boxes of possible objects to be grasped with the probabilities of each gesture. The box closest to the user's gaze is then selected as the object of interest, and the corresponding probabilities will be redirected to the fusion module. The details for each step is provided below.

A. Generalization of the Background

In order for a grasp detector to work properly in a variety of real-life scenarios and in different settings, it is crucial for it to be invariant to the background. Creating such a dataset is an arduous and somewhat impractical task since it requires access to many different locations and settings, and needs the participants and devices to be moved around. Therefore, in recent years, researchers [21], [22] have used more practical solutions such as copy-paste augmentation [23] to tackle this issue. In copy-paste augmentation, using a mask which is usually obtained using a depth camera, the

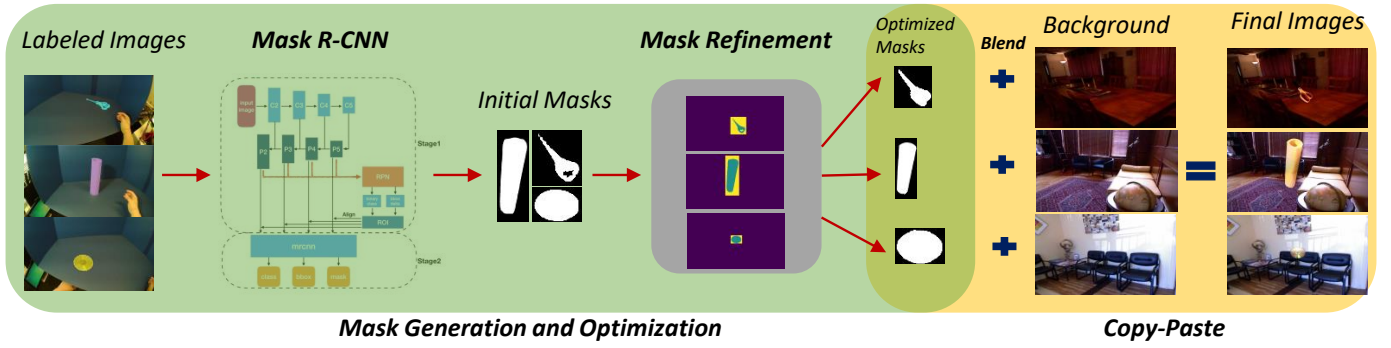


Fig. 7: Overall overview of background generalization using visual mask generation and copy-paste augmentation.

object of interest is copied from the background and pasted into a new background. This work aims to utilize copy-paste augmentation by relying only on the visual data. For this, a screen with a specific color such as blue or green is placed in the experimental environment as the background, and later chroma keying acquires a mask that can separate the foreground from background. Using this mask, the resulting foreground can be superimposed into image data from several places. The overall composition of the proposed copy-paste augmentation pipeline is demonstrated in Figure 7.

1) *Dataset for Background Images*: To have new backgrounds for this superimposition, we found the data from NYU Depth V2 [24] indoor scenes dataset to be very suitable. This dataset consists of images from 464 different, diverse and complex settings i.e., bedrooms, bathrooms, kitchens, home offices, libraries and many more that are captured from a wide range of commercial and residential buildings in three different US cities.

2) *Mask Generation*: During our experiments, we observed that most of the unsupervised computer vision methods which are usually based on color or intensity values fail to separate the foregrounds from the backgrounds correctly. With this intuition in mind, we found that instance segmentation is a more promising and robust method to obtain masks. Because of the simplicity of the task, even when using very few labeled data, retraining Mask R-CNN [25] can provide good enough masks to use in copy-paste augmentation. In our experiments, we labeled 12 images for each of the 53 objects totalling to 636 images. Each of the 12 images were constituted by selecting 2 random images from each of the 6 trials. To prevent overfitting of the network to the very few data at hand, they were heavily augmented using horizontal/vertical flipping, scaling, translation, rotation, blurring, sharpening, Gaussian noise and brightness and contrast changes. Moreover, we used ResNet-101 [26] as the backbone structure.

3) *Refinement of Masks*: Although instance segmentation can provide correct bounding boxes and masks, it is crucial to have a very well defined mask when augmenting data with copy-paste augmentation. As seen in the original work [25], despite the great success of Mask R-CNN in segmenting the objects, a closer look at the masks reveals that the masks do not match the objects' borders perfectly. This usually results in missing pixels in the destination image.

To further refine the masks to have more accurate borders,

we propose to combine Mask R-CNN with GrabCut algorithm [27]. Each mask obtained by Mask R-CNN can be used as a *definite foreground*, while anything outside the bounding box is considered *definite background*. This leaves the pixels inside the bounding box that are not present in the initial mask as *possible foreground*.

4) *Blending*: Due to contrast and lighting differences between the source and destination images, simply copying a foreground image does not result in a seamless final image. To have a seamless blend as the final step for copy-paste augmentation, we use Poisson blending [28]. The refined masks from the previous step are slightly dilated to prevent null gradients. The resulting images are depicted in Figure 8.

Mask generation, refinement and blending provides a pipeline for generalizing the imagery data to enable classification of gestures in different environments. The rest of the augmentation techniques are mentioned in the next subsection accompanied by in-depth analysis of training the grasp detection and classification network.

B. Gesture Detection and Classification

In order to detect the suitable gesture from visual data and control the gesture of the robotic hand, the detector needs to find the box bounding the object and classify the possible gesture. We base our method on YoloV4 [29] that has shown promising results in the domain of object detection. YoloV4 is a fast operating speed object detector optimized for parallel computations in production developed in C++. The architecture of YoloV4 consists of: (i) backbone: CSPDarknet53, (ii) neck: SPP, PAN and (iii) head: YOLOv3. The similarity of MS-COCO dataset [30] which the network is trained on to our dataset makes YoloV4 a suitable source for transfer learning. Moreover, the high throughput of the network when deployed on the GPU will result in real-time detection.

We fine-tune the pre-trained YoloV4 on our dataset using the images augmented by our copy-paste. These images are further generalized by utilizing photometric and geometric distortions and other augmentations from "bag of freebies" [29] i.e., saturation, exposure, hue and mosaicing. To make the network completely invariant to the object's color, we set hue to the maximum value of 1.0 in our experiments. All the training setup are outlined at Table I.

To train, validate and test the network, imagery data has been split based on 4 trials for training and validation and 2



Fig. 8: Three examples of the final images after copy-paste augmentation. Images on the top demonstrate masks before and after refinement. As seen here, mask refinement can significantly improve mask borders and missing parts. Poisson blending can adjust the object being pasted w.r.t. the contrast and brightness of the destination image.

TABLE I: Training Setup

Learning Rate	0.001
Momentum	0.949
Decay	0.0005
Iterations	28680
Batch Size	64
Input Size	$608 \times 608 \times 3$
Angle	0
Saturation	5
Exposure	1.5
Hue	1.0

trials for test, to 48537 (54.1%), 12134 (13.5%) and 29029 (32.3%) images respectively, and balanced according to each class. The augmented data is only used in the training process. Training loss and validation mean average precision (mAP) are outline in Figure 9. To prevent any over-fitting, validation mAP provides a guide on the iteration with the best generalization, reaching 85.43% validation mAP. This results in the very close mAP of 84.97% for the test set, proving the high generalization of the network.

V. MULTIMODAL FUSION OF EMG AND VISION

Previous sections provided independent studies on classification of EMG and visual evidence, with the aim of providing generalized, realistic and accurate inference models for each source of information. Despite these efforts, there exists many contributors for each method to fail in the real world scenarios. To name but a few, EMG evidence would change drastically if any of the electrodes would shift, muscle is fatigued, skin electrode impedance is changed over time or a posture change. On the other hand, the visual information is similarly susceptible to its own artifacts, including object obstruction, lighting changes, etc. Fusion aims to improve robustness of the control method by exploiting multiple sources of information. In this section, we first formulate the proposed fusion method and thereafter, validate and provide our results.

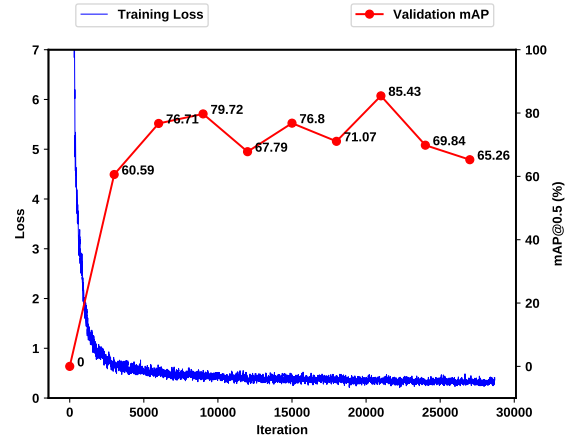


Fig. 9: Training and validation loss (mAP). As the computation time for each mAP calculation will significantly impact the training time of the network, mAP calculations happen every 3000 iterations.

A. Fusion Model

As shown in Figure 10, given the visual information and appearance V of a specific target object, the user first reacts accordingly to the observed V with a designated gesture intent L , and then corresponding muscle activities M of the user are triggered and executed according to the intended gesture comprehended by the user. The purpose of the multimodal fusion between EMG and vision was to maximize the probability of the intended gesture given the collected EMG and vision evidences. Therefore, the optimization of this fusion was formulated by the maximum likelihood problem of object $P(L = \hat{l}|V, M)$, modeled by the graphic model in Figure 10, where V and M are defined as vision evidence and muscle EMG evidence, and L presents the grasp type with optimal decision \hat{l} .

For deriving the optimization object of the multimodal fusion, we wrote down the joint distribution of L , V and M according to the graphic model in Figure 10 as follows:

$$P(L, V, M) = P(M|L)P(L|V)P(V), \quad (1)$$

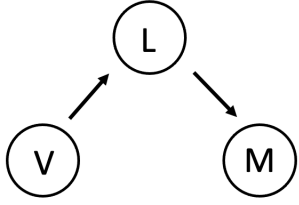


Fig. 10: The graphic model of the multimodal fusion between the EMG and vision evidences.

so the object $P(L = \hat{l}|V, M)$ of the optimization problem can be further written as Eq. (2) according to Eq. (1):

$$\begin{aligned} & \max_{\hat{l} \in \{1, \dots, 13\}} P(L = \hat{l}|V, M) \\ &= \max_{\hat{l} \in \{1, \dots, 13\}} \frac{P(M|L = \hat{l})P(L = \hat{l}|V)P(V)}{P(V, M)}. \end{aligned} \quad (2)$$

Since $P(V)$ and $P(V, M)$ are not functions of variable L and $P(L)$ is evenly distributed over all classes, the optimization object Eq. (2) is equivalent to the following representation

$$\begin{aligned} & \max_{\hat{l} \in \{1, \dots, 13\}} P(M|L = \hat{l})P(L = \hat{l}|V) \\ &= \max_{\hat{l} \in \{1, \dots, 13\}} \frac{P(L = \hat{l}|M)P(M)}{P(L = \hat{l})}P(L = \hat{l}|V) \\ &\sim \max_{\hat{l} \in \{1, \dots, 13\}} P(L = \hat{l}|M)P(L = \hat{l}|V). \end{aligned} \quad (3)$$

The final object of the multimodal fusion is illustrated in Eq. (3), where the optimal estimation \hat{l} of the ground truth should lead to a maximum value of $P(L = \hat{l}|M)P(L = \hat{l}|V)$ among all the 13 grasp types $l \in \{1, \dots, 13\}$. The probability estimators of $P(L = l|M)$ and $P(L = l|V)$ are implemented by the EMG classifier and CNN built in Section III and IV, respectively.

B. Experimental Results

To have a fair comparison of accuracy between EMG and visual classifiers and their resulting fusion, each classifier is trained on the same set of data and tested on data that is unseen to all classifiers. To this end, from the 6 trials belonging to each experiment, 4 has been randomly selected for the training of EMG and visual classifiers and the remaining 2 as the test data. As a result, all of the results presented in this work are based on data unseen to both EMG and visual classifiers.

Figure 11 visualizes the average validation accuracy of EMG, vision and fusion modules over time. The accuracy at each time is defined as the frequency of appearance of the correct label as the maximum probability in a classifier's output probability distribution. We observe that the classification of visual information can perform decently almost at all times and without significant changes except during the grasp phase and some portions of the neighbouring phases where the object is most likely occluded. On the other hand, EMG information can complement this deficiency, given that the subject's hand is mostly active during this phase. This is clearly evident in Figure 11 as the EMG classification

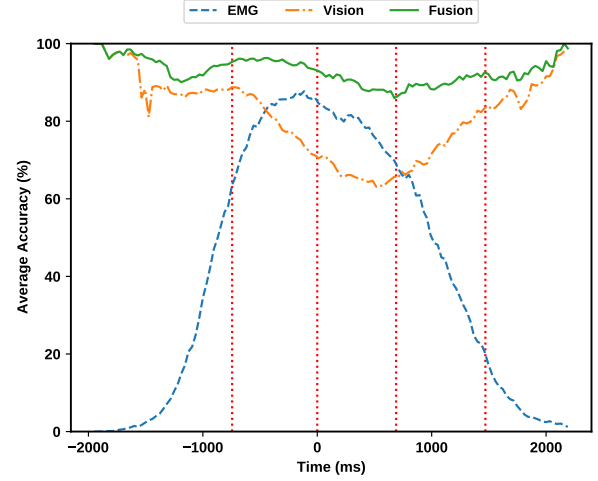


Fig. 11: Average validation accuracy. Note that the predictions from each source generally complements the other source. Fusing EMG and visual evidence has improved the overall accuracy and robustness of the estimation.

TABLE II: Accuracy of each module during different phases in percentage. Reach phase is demonstrated in bold, as is the most critical phase for decision making. Note that a random classifier has a $\frac{1}{13} = 7.7\%$ chance for each class.

	Phase					Total
	Rest	Reach	Grasp	Return	Rest	
EMG	16.86	81.64	78.66	45.41	6.33	41.85
Vision	90.69	80.5	66.22	74.05	88.59	81.46
Fusion	94.89	95.3	89.7	89.81	93.31	92.93

outperform visual classifier. The complementary characteristic of EMG and visual information is also noticeable at rest phases where the subject's hand is least active. During resting, the object of interest is clearly visible by camera, therefore resulting in high accuracy of the visual classifier.

In addition to this complementary behaviour, fusion is always outperforming each individual classifier. This means that fusion can add additional robustness even when both sources provide enough information for a correct decision. To provide more details, the summary of each module's accuracy is provided in Table II in different phases.

Having a robust control of the grasp type at all times is essential especially at reaching phase, where the actual grasping decision is sent to the robot's actuators. Fusion of visual and EMG evidence enables robust classification of grasp types, giving the robotic hand enough time to perform the grasp. Moreover, we recommend utilizing robot control policy to exploit past decisions into their fusion based on their system configurations and constraints, as our experiments show that by simply smoothing fusion decisions, the average accuracy is further increased to the significant value of 96.8%. We suggest that future studies can also utilize more sophisticated methods based on machine learning and deep learners for fusion of the information.

VI. CONCLUSION

For robotic prosthetic hands to effectively compensate for the lost ability of lower arm amputees during daily life activities, control of the hand must be intuitive and robust to missing and sometimes inaccurate sensor data. Solely relying on one source of information e.g., EMG or vision, is prone to poor performance due specific drawbacks of each source. Hence a shift in the approach to one that fuses multiple sources of information is required. In this work we collected a dataset of synchronized EMG and visual data of daily objects and provided details on our proposed process for sensor fusion including EMG segmentation and gesture classification and camera-based grasp detection that is bundled with background generalization using copy-paste augmentation. Based on a graphical model, we represented the multimodal fusion as a maximum likelihood problem to increase robotic control accuracy and robustness.

In our experiments, we observed the complementary behaviour of visual and EMG data. EMG generally performs better when reaching and grasping an object when the imagery data cannot provide useful information due to occlusion. Visual information can provide information about the needed grasp prior to movement, when EMG is unavailable. Our experiments show that fusion always outperforms each individual classifier demonstrating that fusion can add additional robustness even when both sources provide enough information for a grasp decision. We observe that fusion improves the average grasp classification accuracy while at reaching phase by 13.66%, and 14.8% for EMG and visual classification respectively with the total accuracy of 95.3%.

ACKNOWLEDGMENT

This work is partially supported by NSF (CPS-1544895, CPS-1544636, CPS-1544815).

REFERENCES

- [1] K. Ziegler-Graham, E. J. MacKenzie, P. L. Ephraim, T. G. Trivison, and R. Brookmeyer, "Estimating the prevalence of limb loss in the united states: 2005 to 2050," *Archives of Physical Medicine and Rehabilitation*, vol. 89, no. 3, pp. 422–429, 2008.
- [2] C. H. Jang, H. S. Yang, H. E. Yang, S. Y. Lee, J. W. Kwon, B. D. Yun, J. Y. Choi, S. N. Kim, and H. W. Jeong, "A survey on activities of daily living and occupations of upper extremity amputees," *Annals of rehabilitation medicine*, vol. 35, no. 6, p. 907, 2011.
- [3] J.-H. Cho, J.-R. Jeong, D.-J. Kim, and S.-W. Lee, "A novel approach to classify natural grasp actions by estimating muscle activity patterns from eeg signals," in *2020 8th international winter conference on brain-computer interface (BCI)*. IEEE, 2020, pp. 1–4.
- [4] S. Y. Günay, F. Quivira, and D. Erdoğan, "Muscle synergy-based grasp classification for robotic hand prosthetics," in *Proceedings of the 10th international conference on pervasive technologies related to assistive environments*, 2017, pp. 335–338.
- [5] S. Bitzer and P. Van Der Smagt, "Learning emg control of a robotic hand: towards active prostheses," in *Proceedings 2006 IEEE International Conference on Robotics and Automation, 2006. ICRA 2006*. IEEE, 2006, pp. 2819–2823.
- [6] M. Hakonen, H. Piitulainen, and A. Visala, "Current state of digital signal processing in myoelectric interfaces and related applications," *Biomedical Signal Processing and Control*, vol. 18, pp. 334–359, 2015.
- [7] H.-J. Hwang, J. M. Hahne, and K.-R. Müller, "Real-time robustness evaluation of regression based myoelectric control against arm position change and donning/doffing," *PloS one*, vol. 12, no. 11, p. e0186318, 2017.
- [8] M. Kassner, W. Patera, and A. Bulling, "Pupil: an open source platform for pervasive eye tracking and mobile gaze-based interaction," in *Proceedings of the 2014 ACM international joint conference on pervasive and ubiquitous computing: Adjunct publication*, 2014, pp. 1151–1160.
- [9] A. Zaharescu, "An object grasping literature survey in computer vision and robotics," 2005.
- [10] M. Han, S. Y. Günay, G. Schirner, T. Padi, and D. Erdoğan, "Hands: a multimodal dataset for modeling toward human grasp intent inference in prosthetic hands," *Intelligent service robotics*, vol. 13, no. 1, pp. 179–185, 2020.
- [11] iMatix, "Zeromq," <https://github.com/zeromq/libzmq>, 2021.
- [12] T. Feix, J. Romero, H.-B. Schmiedmayer, A. M. Dollar, and D. Kragic, "The grasp taxonomy of human grasp types," *IEEE Transactions on Human-Machine Systems*, vol. 46, no. 1, pp. 66–77, 2016.
- [13] L. Resnik, S. L. Klinger, and K. Etter, "The deka arm: Its features, functionality, and evolution during the veterans affairs study to optimize the deka arm," *Prosthetics and orthotics international*, vol. 38, no. 6, pp. 492–504, 2014.
- [14] N. Hogan and R. W. Mann, "Myoelectric signal processing: Optimal estimation applied to electromyography-part i: Derivation of the optimal myoprocessor," *IEEE Transactions on Biomedical Engineering*, no. 7, pp. 382–395, 1980.
- [15] F. P. Kendall, E. K. McCreary, P. Provance, M. Rodgers, and W. Romani, "Muscles: Testing and function, with posture and pain (kendall, muscles)," *LWW*, 2005.
- [16] A. Phinyomark, P. Phukpattaranont, and C. Limsakul, "Feature reduction and selection for emg signal classification," *Expert systems with applications*, vol. 39, no. 8, pp. 7420–7431, 2012.
- [17] D. Hallac, P. Nystrup, and S. Boyd, "Greedy gaussian segmentation of multivariate time series," *Advances in Data Analysis and Classification*, vol. 13, no. 3, pp. 727–751, 2019.
- [18] E. A. Clancy and N. Hogan, "Probability density of the surface electromyogram and its relation to amplitude detectors," *IEEE Transactions on Biomedical Engineering*, vol. 46, no. 6, pp. 730–739, 1999.
- [19] M. Jeannerod, "The timing of natural prehension movements," *Journal of motor behavior*, vol. 16, no. 3, pp. 235–254, 1984.
- [20] P. Geurts, D. Ernst, and L. Wehenkel, "Extremely randomized trees," *Machine learning*, vol. 63, no. 1, pp. 3–42, 2006.
- [21] T. Chalasani, J. Ondrej, and A. Smolic, "Egocentric gesture recognition for head-mounted ar devices," in *2018 IEEE International Symposium on Mixed and Augmented Reality Adjunct (ISMAR-Adjunct)*. IEEE, 2018, pp. 109–114.
- [22] G. Georgakis, A. Mousavian, A. C. Berg, and J. Kosecka, "Synthesizing training data for object detection in indoor scenes," *arXiv preprint arXiv:1702.07836*, 2017.
- [23] G. Ghiasi, Y. Cui, A. Srinivas, R. Qian, T.-Y. Lin, E. D. Cubuk, Q. V. Le, and B. Zoph, "Simple copy-paste is a strong data augmentation method for instance segmentation," *arXiv preprint arXiv:2012.07177*, 2020.
- [24] P. K. Nathan Silberman, Derek Hoiem and R. Fergus, "Indoor segmentation and support inference from rgb-d images," in *ECCV*, 2012.
- [25] K. He, G. Gkioxari, P. Dollár, and R. Girshick, "Mask r-cnn," in *Proceedings of the IEEE international conference on computer vision*, 2017, pp. 2961–2969.
- [26] K. He, X. Zhang, S. Ren, and J. Sun, "Deep residual learning for image recognition," in *Proceedings of the IEEE conference on computer vision and pattern recognition*, 2016, pp. 770–778.
- [27] C. Rother, V. Kolmogorov, and A. Blake, "“grabcut” interactive foreground extraction using iterated graph cuts," *ACM transactions on graphics (TOG)*, vol. 23, no. 3, pp. 309–314, 2004.
- [28] P. Pérez, M. Gangnet, and A. Blake, "Poisson image editing," in *ACM SIGGRAPH 2003 Papers*, 2003, pp. 313–318.
- [29] A. Bochkovskiy, C.-Y. Wang, and H.-Y. M. Liao, "Yolov4: Optimal speed and accuracy of object detection," *arXiv preprint arXiv:2004.10934*, 2020.
- [30] T.-Y. Lin, M. Maire, S. Belongie, J. Hays, P. Perona, D. Ramanan, P. Dollár, and C. L. Zitnick, "Microsoft coco: Common objects in context," in *European conference on computer vision*. Springer, 2014, pp. 740–755.